Proceedings of the 2024 Winter Simulation Conference
H. Lam, E. Azar, D. Batur, S. Gao, W. Xie, S. R. Hunter, and M. D. Rossetti, eds.

SPLINE INTERPOLATION-BASED MULTI-SCALE MODEL FOR ETCHING IN A CHLORINE-ARGON INDUCTIVELY COUPLED PLASMA

Lado Filipovic[1], and Tobias Reiter[1]

[1]CDL for Multi-Scale Process Modeling of Semiconductor Devices and Sensors at the Institute for Microelectronics, TU Wien, 1040 Vienna, AUSTRIA

ABSTRACT

A multi-variable spline interpolation is used in order to quickly obtain the wafer incident fluxes from inside an inductively coupled plasma chamber with a chlorine and argon chemistry. The data is obtained by performing a total of 18 750 chamber simulations while varying the inputs which include the inductive coil power, the gas flow rate, the chamber pressure, the chlorine gas concentration ratio, the temperature, and the applied bias voltage. The data is used to generate a six-dimensional hypercube for each flux of interest where each dimension corresponds to one of the varied parameters. The fluxes are then incorporated into a semi-empirical feature scale plasma etching model in the process simulation tool ViennaPS. The chemical sticking coefficient is derived from measurements and the model includes the etch rate resulting from the chemical etch component, ion sputtering, and ion-enhanced etching.

1 INTRODUCTION

A fundamental processing step for the fabrication of semiconductor devices is plasma etching (Huff 2021; Krüger et al. 2024). In particular, the patterning of metal-nitrides such as TiN and AlN has been frequently performed using an inductively coupled plasma (ICP) with chlorine and argon gases (Kim et al. 2011; Woo et al. 2011; Lee Sang et al. 2015; Woo et al. 2022). ICP is a means to deliver power to the electrons without the need for elevated temperatures. The electrons then initiate collisions with gas molecules, resulting in the formation of neutral radical species and charged ions (Hori 2022). These two types of species are mainly responsible for surface interactions and ultimate material removal.

1.1 Species Involved in Plasma Etching

Neutral radicals interact chemically with the surface, resulting in an isotropic profile. Their movement inside the chamber and through the wafer features is primarily governed by diffusion. In the reactor, their diffusive motion is governed by collisions with other species. However, once they reach the feature scale region, interactions with the substrate's features are much more frequent than inter-particle collisions. Therefore, their motion is governed by reflections from the feature sidewalls, commonly referred to as Knudsen diffusion (Reiter et al. 2024). The ability for the radical particles to reach all sections of the feature in order to initiate an etching reaction rests primarily on the sticking coefficient γ. The sticking coefficient is a parameter which determines how frequently an interaction between a particle and the surface will result in that particle being adsorbed, contributing to the surface coverage of said particle. Once it is absorbed, the chemical surface reaction rates determine the next steps, mainly the possible removal of the surface atoms, weakening of the bonds near the substrate surface, or re-deposition (Donnelly and Kornblit 2013; Klemenschits et al. 2018; Bobinac et al. 2023). Infrequent adsorption means that many particles will reflect from the surface and diffuse deep into high aspect ratio (HAR) structures. However, a small sticking coefficient also means a very slow etch rate.

The benefit of radical-driven etching lies in the potential for making the process highly selective. Since the surface reactions are chemical in nature, by using a proper mix of radical species, the etch process can

be tailored to be highly specific towards a desired film (Huang et al. 2015; Osipov et al. 2023). Unlike neutral radicals, which mainly diffuse, the movement of charged ions inside the chamber is governed by the applied electric field which typically ensures that positively charged ions are accelerated towards the wafer surface. Once the ions strike the wafer with a specific energy, they sputter surface atoms away. Since the electric field is directional, the ion movements are also much more directional than radicals, which is why pure ion etching mainly produces anisotropic profiles (Donnelly and Kornblit 2013). The benefit of ion sputtering lies in precisely this ability to generate anisotropic etch profiles, which are particularly important for high aspect ratio (HAR) structures (Krüger et al. 2024; Manstetten et al. 2017).

1.2 Modeling Plasma Etching

Technology computer aided design (TCAD) has evolved significantly, becoming essential for micro- and nanoelectronics advancement. Yet, traditional models still struggle to capture different size and time scales comprehensively and efficiently. In particular, there is a divide when it comes to modeling plasma etching at the equipment scale or process TCAD at the feature scale, where the topography movement is simulated (Klemenschits et al. 2018). The large gap between the real equipment behavior and the available simulations is what is keeping many fabrication companies from fully integrating process TCAD - especially topography simulations - in their designs on a very large scale. The gold standard for the design of new architectures and geometries still hinges in large part on going into the clean room and operating time consuming, power-hungry, and environmentally unfriendly equipment.

Figure 1 depicts a schematic of the scales in question. In the reactor scale, the particles diffuse by striking against each other. However, at the feature scale, the mean free path of particles is mainly governed by the distance between their reflections off the feature sidewalls: This is especially true at the nano-scale. The mean free path λ_r in the reactor is meant to follow the theory of a free gas

$$\lambda_r = \frac{k_B T}{\sqrt{2}\pi d_m^2 p},$$

where k_B is the Boltzmann constant, T is temperature, d_m is the effective diameter of the gas molecule, and p is the pressure. Depending on these conditions, the mean free path can vary from about 100 micrometers to several millimeters (Ertl 2010).

Therefore, in the feature scale, which is the region of interest for process TCAD, the particles are assumed to move in straight lines and Monte Carlo ray tracing is employed to count how many particles reach each section of the feature during a time step. In order to merge the reactor and feature scales, a virtual source plane is applied which is meant to represent the flux of particles from the reactor which enter the feature scale. The neutral particles are initiated from the source plane following a cosine distribution, which best replicates the Maxwell-Boltzmann behavior of the particles inside the chamber (Greenwood 2002; Ertl 2010). The ions, on the other hand, are more directional, due to their movement being governed by the applied electric field. They follow a power cosine distribution (Ertl 2010).

2 TITANIUM NITRIDE PLASMA ETCHING MODEL

As noted in the previous section, feature-scale plasma etching models assume ballistic transport of particles at feature-scale and Langmuir-type adsorption (Ertl 2010). The inputs to the feature-scale simulations are the initial substrate topography, including material information such as the geometry of the mask layer, and the particles which leave the source plane. The flux of particles, as well as their direction and energy - in the case of ions - can be obtained from chamber simulations (or experiments). The surfaces are typically represented using implicit data structures, such as the signed distance function (SDF) due to several benefits this provides (Klemenschits et al. 2018). Explicit surface representations, such as triangular meshes, require frequent re-meshing due to surface evolution and the unavoidable formation of low-quality mesh elements once the nodes of the surface element are stretched inward or outward (Bobinac et al. 2023). Using an

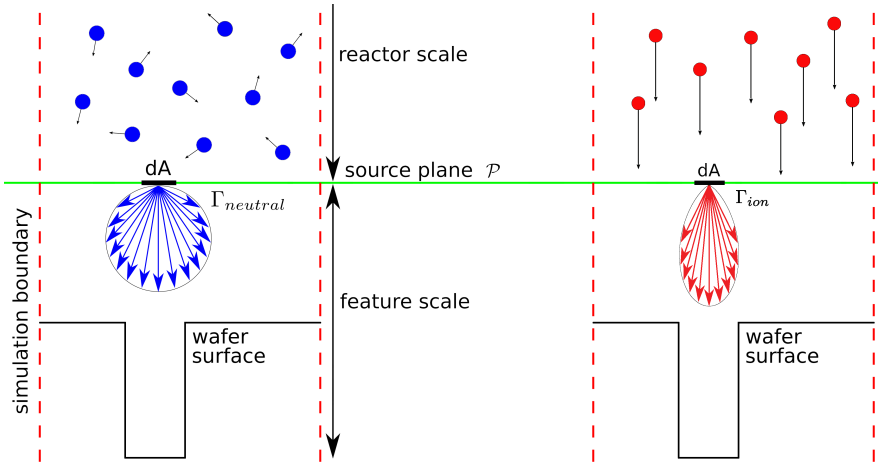

Figure 1: Scales of particle transport for (left) neutral radicals and (right) charged ions in an electric field. The scale above the source plane refers to the reactor scale, where transport is governed by inter-particle reactions. Below the source plane, in the feature-scale region, interactions with the sidewalls dominate.

SDF and moving the surface by solving the level set equation is a method by which the problems with meshes can be overcome during topography evolution (Ertl and Selberherr 2009).

2.1 Level Set Surface Representation

To simulate plasma etching, multiple materials and their interfaces must first be defined, a task facilitated by the level set approach. To model the impact of atoms, molecules, and ions on the surface, we utilize particles, with each particle in the simulation representing several hundred to several thousand real-world radicals or ions. Their movement within the chamber, particularly in proximity to the wafer surface, is modeled using ray tracing. At the intersection of a particle ray and the surface, the surface kinetics model, encompassing processes like sputtering, chemical etching, re-deposition, and reflection, is then applied. This approach follows the conventional top-down Monte Carlo ray tracing, shown in Figure 2 (Ertl and Selberherr 2009; Ertl 2010; Klemenschits et al. 2018; Klemenschits 2022; Bobinac et al. 2023).

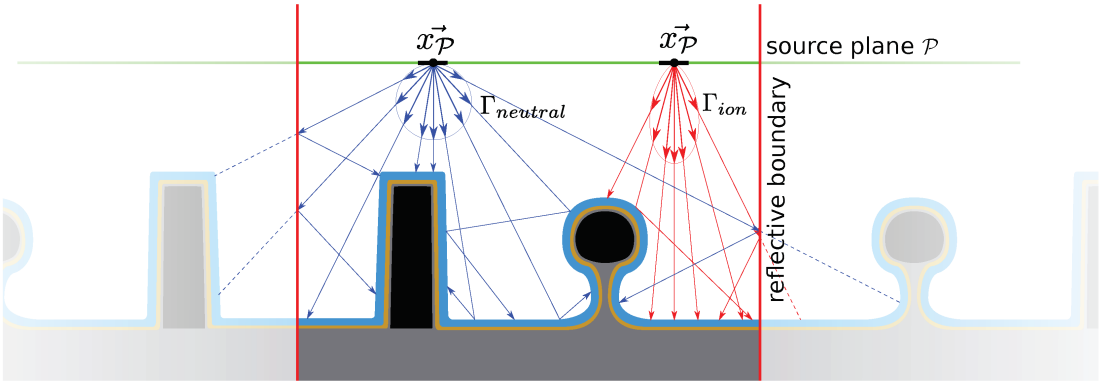

Figure 2: Schematic depiction of top-down Monte Carlo ray tracing of particles (neutral radicals - blue, ions - red) from the source plane to the surface. Coned specular reflections are applied for reflected ions, while diffuse reflections are used for neutral species.

The surfaces are described by an SDF $\phi(\vec{x})$ defined at all points in space (Bloomenthal et al. 1997; Sethian 1999) on a Cartesian grid with signed distance values provided at each point. The true location of the surface is then at the implicit contour where the SDF is equal to a specific scalar value, typically zero. The SDF $\phi(\vec{x})$ is constructed based on the signed distance d of a domain point $\vec{x}$ from the surface S bounding the volume M

$$\phi(\vec{x}) = \begin{cases} -d, & \vec{x} \in M \\ 0, & \vec{x} \in S \\ d, & \vec{x} \notin M \end{cases}.$$

The sign of $\phi(\vec{x})$ indicates whether the point is inside or outside of the volume M. The time evolution of the surface is given by the surface velocity along the normal direction $v(\vec{x})$ For a geometry with non-constant SDF gradients, the level set equation becomes:

$$\frac{\delta\phi(\vec{x},t)}{\delta t} + v(\vec{x})\,|\nabla\phi(\vec{x},t)| = 0,$$

which is a form of the Hamilton-Jacobi equations that can be solved using finite difference schemes (Osher and Sethian 1988; Osher and Shu 1991). The surface velocity is applied to update the SDF $\phi(\vec{x})$, stored at the points defined on a regular grid. The movement of the surface is then recorded through a change in the SDF values (Klemenschits et al. 2018). We have released an open-source level set framework ViennaLS to represent the surfaces for these types of problems (Reiter et al. 2024a).

2.2 Surface Kinetics Model

To model the evolution of the surface in time during Cl_2/Ar plasma etching, we must calculate the surface velocity $v(\vec{x})$ at all grid points $\vec{x}$ while considering the fluxes of chlorine (Cl) radicals and positively-charged ions (Cl^+, Cl_2^+, and Ar^+) as they impinge on the substrate surface. Several simulation steps are executed during each time step:

- Ray tracing is applied to calculate the impingement rates, or relative flux, along the entire feature surface, assuming a known flux from the source plane and a predetermined sticking coefficient. For this, we apply our in-house open-source ray tracing framework ViennaRay (Reiter et al. 2024b).
- The flux is used to compute the surface coverages or adsorption of all relevant species which are stored on the surface points. For the Cl_2/Ar plasma, the required coverage is of Cl radicals.
- The surface etch rate is calculated based on the impingement rates and coverages.
- The surface etch rate is then extended to calculate the effective velocities $v(\vec{x})$ at all defined level set points in space $\vec{x}$, which are used when solving the level set equation.

The final etch rate is comprised of three components, including chemical etching, physical sputtering, and ion-enhanced etching:

1. Chemical etching: The chlorine radical reacts with the surface TiN, breaking the bond and creating byproducts $TiCl_x$ and NCl_x (Tonotani et al. 2003). The chemical reaction which governs one such removal of byproduct is given by

$$TiN_{(s)} + 2Cl_{2(g)} \rightarrow TiCl_{4(g)} + 0.5N_{2(g)}.$$

2. Physical sputtering: The ions in the chamber, when accelerated in the sheath potential, will strike the silicon surface with an energy which is directly proportional to the applied bias. This will result in material removal, assuming that the ion's energy E is above the TiN threshold E_{th}. The sputtering yield depends on the ion energy and incidence angle θ according to (Steinbrüchel 1989;

Klein and Ramirez 2000):

$$Y(E,\theta) = \left(\sqrt{E} - \sqrt{E_{th}}\right) f(\theta),$$

where $f(\theta)$ is a material-dependent angular yield function for which often an empirical approximation is used (Matsunami et al. 1984).

3. Ion-enhanced etching: Chlorine-saturated surfaces are more prone to being physically sputtered, meaning that the threshold energy to sputtering is reduced. In addition, the angle dependence of ion-enhanced etching depends greatly on the ion energy (Shumilov et al. 2016).

Therefore, the feature-scale model should trace Cl and ion species in the feature scale, store the Cl coverages on the surface, and use this coverage and ion flux to derive the surface rate. This calculation and implementation of the Cl_2/Ar etching model of TiN is implemented in the in-house open-source framework ViennaPS (Reiter et al. 2024). The coverages of chlorine on the silicon surface, given by θ_{Cl}, are calculated using a Langmuir–Hinshelwood-type surface site balance equation which is given by (Cooperberg et al. 2002):

$$\sigma_{TiN}\frac{d\theta_{Cl}}{dt} = \gamma_{Cl}\Gamma_{Cl}(1-\theta_{Cl}) - k\sigma_{TiN}\theta_{Cl} - 2Y_{ie}\Gamma_i\theta_{Cl}. \tag{1}$$

Here, Γ_{Cl} and Γ_i are the chlorine and ion fluxes, respectively; γ_{Cl} is the sticking coefficient for chlorine on a clean TiN surface; σ_{TiN} is the surface site density of TiN molecular units; k is the TiN chemical etching coefficient, and Y_{ie} is the total ion-enhanced etching rate, which is linked to the ion energies in the reactor (Ertl 2010).

Assuming steady-state conditions, Equations (1) can be set to zero, resulting in the following expression for the TiN surface coverage by chlorine:

$$\theta_{Cl} = \frac{\gamma_{Cl}\Gamma_{Cl}}{\gamma_{Cl}\Gamma_{Cl} + k\sigma_{TiN} + 2Y_{ie}\Gamma_i}.$$

The steady-state can be assumed here since the incoming fluxes are on the order of 10^{16}–$10^{19}\,\mathrm{cm^{-2}s^{-1}}$, which is much faster than the surface velocity, which is on the order of several nanometers per second (Chiu et al. 2001; Woo et al. 2011; Woo et al. 2022). Finally, the surface etch rate is given by

$$\mathrm{ER} = \frac{1}{\rho_{TiN}}\left(k\sigma_{TiN}\theta_{Cl} + Y_p\Gamma_i + Y_{ie}\Gamma_i\theta_{Cl}\right), \tag{2}$$

where ρ_{TiN} is the density of TiN. The first, second, and third terms in the brackets of Equation (2) reflect the chemical etching, physical sputtering, and ion-enhanced etch components, described above. A schematic representation of the modeled particle-surface interactions is provided in Figure 3.

2.3 Chemical Etch Rate Components

In order to calculate the sticking coefficient, we can either perform *ab-initio* calculations (Alao et al. 2022), carry out simulations of the surface chemical reactions (Shumilov et al. 2016), or calibrate the value with experimental measurements (Silbey et al. 2022). If we ignore the ion flux, meaning that we perform an etching step on a flat wafer while the electric field is turned off, according to equation (2) the etch rate will be fully dependent on the chlorine flux Γ_{Cl} and sticking coefficient γ_{Cl}. Therefore, if we can experimentally determine the etch rate while the chamber conditions which were applied to generate this rate are known, such as gas composition, pressure, and temperature, we can derive the sticking coefficient (Silbey et al. 2022):

$$\gamma_{Cl} = \frac{r_{TiN}\rho_{TiN}}{M_{TiN}p}\sqrt{2RTM_{Cl}}, \tag{3}$$

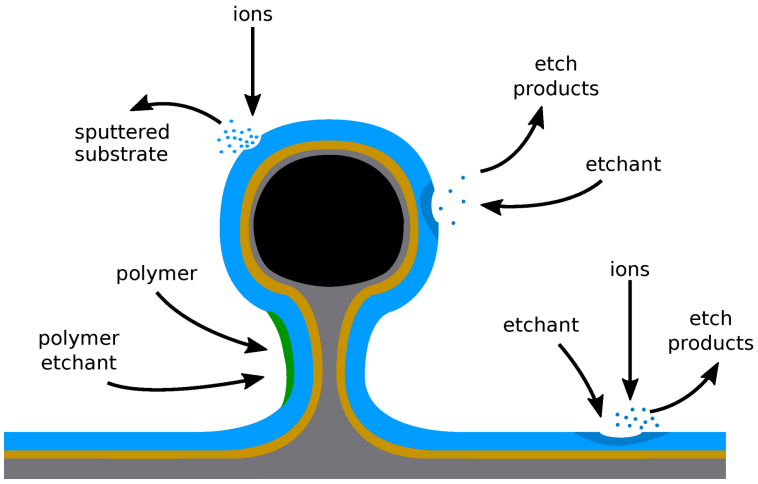

Figure 3: Physical processes considered during plasma etching. Passivating species inhibit chemical etching at the sidewalls, ion bombardment removes material from the substrate by physical sputtering, chemical etching removes material by forming volatile etch products, and ion-enhanced etching speeds up this process by breaking existing bonds, enhancing the formation of volatile etch products.

where r_{TiN} is the measured etch rate, R is the universal gas constant, and M_x are the molar masses of species x. When we apply this equation to the etch rate of 6.83 nm/s obtained at a pressure of 0.013 mbarr and temperature of 45 °C by Woo et al. (Woo et al. 2011), a sticking coefficient of $\gamma_{Cl} = 0.00628$ is calculated. This value is in a range which is quite typical for highly conformal processes. However, as can be observed from Equation (3) this value can change as the pressure and temperature in the chamber is varied.

Furthermore, to calculate the TiN chemical etching constant, we use the saturation etch rate of 410 nm/s from Woo et al. (2011) and use the discussion from Cooperberg et al. (2002) to derive a k value of 16.5 s^{-1}, where

$$k = \frac{R_{sat}\rho_{TiN}}{\sigma_{TiN}M_{TiN}},$$

with the surface site density of TiN being $\sigma_{TiN} = 3.61 \times 10^{-9}$ mol/cm^2 (Grujicic and Lai 2001). The ion energy distribution can be derived from the sheath potential V_{sheath}, which is a sum of the plasma potential V_p and applied bias V_{bias} (Panagopoulos and Economou 1999).

2.4 Model Parameters Summary

In order to perform physical etching simulations in a Cl_2/Ar plasma, we need to find several parameters, which can be extracted from measurements, calculated using chamber-level simulations, or a combination of the two. A summary of the required parameters, their meaning, and their source is provided in Table 1. In principle, the parameters we aim to obtain from chamber simulations are the fluxes of neutral radical Cl and ions immediately above the wafer surface.

2.5 Inductively Coupled Plasma Chamber Model

In order to calculate the ion and neutral fluxes under a wide range of inductively coupled plasma chamber conditions, we use the COMSOL Multiphysics® 2024 finite element software. The primary goal was to model the Cl_2/Ar plasma while varying the coil power, gas flow rate, gas composition ratio between Cl_2 and Ar, chamber pressure, temperature, and the bias voltage. A schematic view of the chamber used in this study is shown in Figure 4. As can be observed from the discussion in Section 2.2, the feature scale model typically uses parameters which are not immediately linked to equipment conditions. This makes it difficult

Table 1: Summary of relevant parameters for the feature-scale model and their sources.

Parameter	Description	Source
σ_{TiN}	TiN surface site density (mol/cm^2)	Derived from bulk - 3.61×10^{-9}
k	TiN chemical etching coefficient (s^{-1})	Derived from measurement - 16.52
Γ_i	Ion flux ($cm^{-2}s^{-1}$)	Chamber simulation
Γ_{Cl}	Cl etchant flux ($cm^{-2}s^{-1}$)	Chamber simulation
γ_{Cl}	Cl sticking coefficient	Derived from measurement - 0.00628
E_{th}	TiN sputtering threshold (eV)	Typical value of about 20
E_{ie}	TiN ion-enhanced etching threshold (eV)	Typical value of about 5
E	Mean ion energy	Derived from sheath potential
Y_p	Yield function for sputtering	Empirical from Shumilov et al. (2016)
Y_{ie}	Yield function for ion-enhanced etching	Empirical from Shumilov et al. (2016)

to perform equipment variability studies or to use feature-scale simulations to calibrate the equipment for a particular process. For this reason, a link between the feature-scale model parameters, such as the flux, and the chamber settings is required. Therefore, the main purpose of the chamber simulations in this study is to use them to devise a feature-scale model which takes equipment settings as an input.

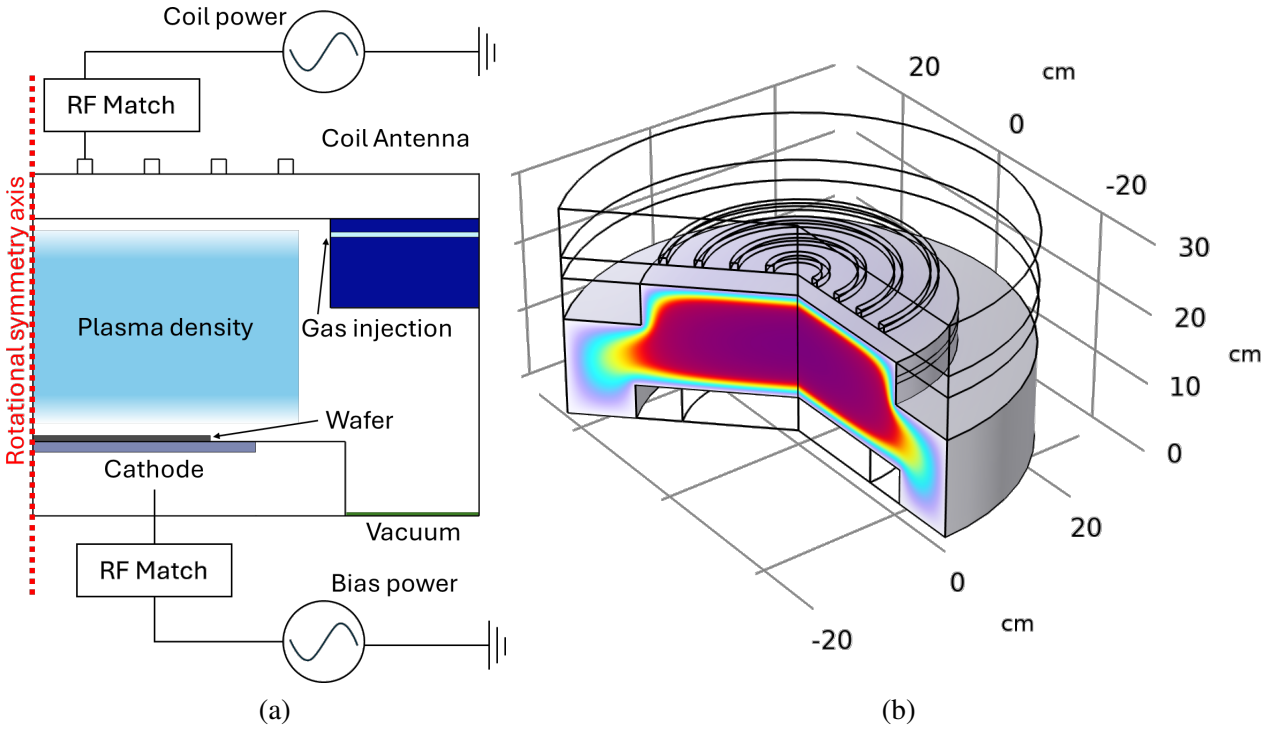

Figure 4: Schematic diagram of the inductively coupled plasma system (a) in two dimensions with rotational symmetry and (b) in three dimensions.

The plasma is generated by first applying electric power to the coils which generate a strong magnetic field inside the chamber. This magnetic field induces high-energy electrons therein. The gases, which are a combination of Cl_2 and Ar are then introduced into the chamber through the nozzle with a desired flow rate. The collisions between the gases and high-energy electrons lead to several possible reactions. The plasma chemistry used for this study includes electron impact reactions from the electron momentum transfer cross sections provided by the SIGLO database (SIGLO database 2023) released as part of the

Plasma Data Exchange Project and the LXCat website (Carbone et al. 2021). We performed chamber simulations while varying the input conditions as follows:

Coil power P_{coil} (W):	200,	300,	400,	500,	600	
Gas flow Q_f (sccm):	50,	75,	100,	125,	150	
Pressure p (Torr):	0.007,	0.01,	0.013,	0.016,	0.019	
Cl_2 concentration ratio:	0.55,	0.65,	0.75,	0.85,	0.95	
Temperature T (°C):	25,	35,	45,	55,	65	
Bias voltage V_{bias} (V):	0,	-30,	-60,	-90,	-120,	-150

Running all the combinations amounts to a total of 18 750 different input conditions which are simulated. For all tested cases, the plasma potential was found to be in the range of 14 V to 17 V. From each calculation, the relevant radical and ion fluxes at the center of the chamber are stored. These fluxes can then be used directly as input to the feature-scale model. However, performing a chamber-scale simulation followed by a feature-scale simulation every time is time consuming and can lead to convergence issues. It also introduces a layer of complexity to the data structures and computational processess typically applied for process TCAD simulations. Instead, we use the compiled data to create a multi-variable spline interpolation model to replace the chamber simulation and to provide a link to equipment settings instead of fluxes as inputs to the feature-scale topography simulation. Since the model is not geometry-specific and is based on a physical or semi-empirical simulation approach, this method allows to investigate different masks and features under realistic chamber conditions.

3 MULTI-SCALE INTERPOLATIVE MODEL

3.1 Multi-Variable Spline Interpolation

From the chamber simulations, the fluxes of ions and radicals are stored in a hexeract - a six dimensional hypercube - where each dimension refers to one of the chamber inputs which were varied. The hexeract is then used to build a multi-variable spline interpolation model in order to allow to interpolate chamber conditions between the simulated values. This approach, visualized in Figure 5, allows to populate the feature-scale etching model with the entire simulation space while the user never needs to calculate or know the exact value of the flux on the top of the wafer. The grey arrows in Figure 5 show the training and creation of the hypercube, while the green arrows show the simulation flow which uses the multi-variable spline model. When using the model, the spline of order 1 shows a good balance between the speed required to calculate intermediate values and the accuracy of the interpolative prediction. For a piecewise linear spline (order 1) the interpolated values for the fluxes are calculated in less than one millisecond, while using splines of a higher order is more complex and requires several minutes.

3.2 Combined Reactor- and Feature-Scale Simulation

To show the application of the multi-scale interpolative model, the model for Cl_2/Ar etching described in Section 2.2 was updated to replace the ion and chlorine fluxes with functions from the interpolation f_i:

$$\Gamma_x = f_{i,x}\left(P_{coil}, Q_{sccm}, p, \frac{C_{Cl_2}}{C_{Cl_2}+C_{Ar}}, T, V_{bias}\right),$$

where x is either a Cl radical, an Ar^+ ion, a Cl^+ ion, or a Cl_2^+ ion. The ion flux is then the sum of all positively charged ions taking part in sputtering:

$$\Gamma_i = \Gamma_{Ar^+} + \Gamma_{Cl^+} + \Gamma_{Cl_2^+}.$$

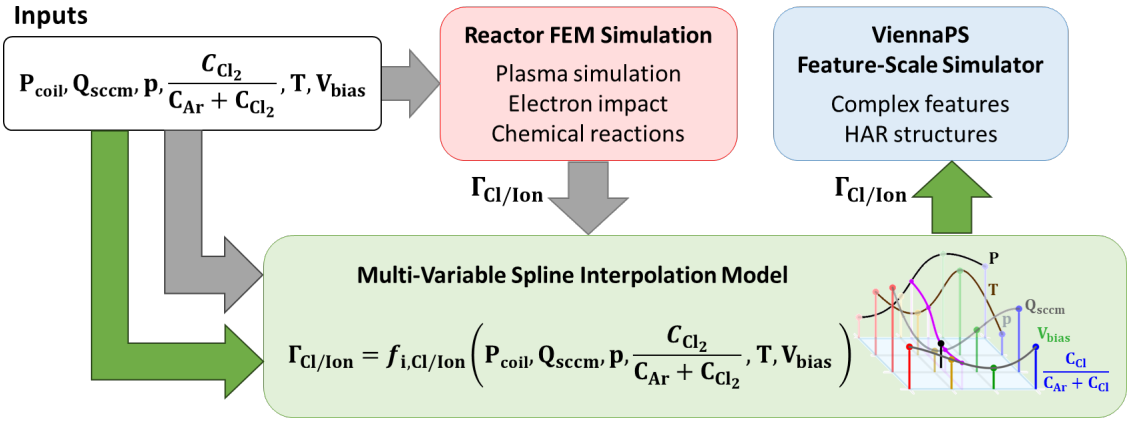

Figure 5: Implementation of a multi-scale plasma etch model using multi-variable spline interpolation.

We use the developed approach to simulate several etched profiles through a cylindrical SiO_2 mask with a height of 120 μm, a top diameter of 35 μm, and a sidewall tapering of 2°. The inputs of the plasma chamber are chosen at random to compile four structures, shown in Table 2 with results shown in Figure 6.

Table 2: Randomly generated input values for the Cl_2/Ar chamber which are applied to the equipment-informed feature-scale etching model in ViennaPS.

Parameter	Structure A	Structure B	Structure C	Structure D
P_{coil} (W)	550.4	242.4	450.4	481.8
Q_f (sccm)	62.4	115.5	89.4	57.7
p (mTorr)	0.0188	0.0129	0.0126	0.0154
$C_{Cl_2}/(C_{Cl_2}+C_{Ar})$	0.896	0.611	0.912	0.600
T °C	55.1	55.2	63.1	35.9
V_{bias} (V)	-119.7	-2.3	-71.2	-117.9

The results of the simulations of the different structures are shown in Figure 6. From these, we can already note some expected behavior. For example, increasing the coil power increases the plasma density, leading to more chemical etching, which can be observed by an increase in the profile depths and widths. Increasing the gas flow should also lead to higher fluxes; however, in the case of structure B, where the gas flow is almost double that of structure A, the simultaneous reduction in the Cl_2 concentration results in less chemical etching compared to Structure A. The lack of an applied bias also means that ions do not have sufficient energy to provide a vertical etch component. Overall, the results are in qualitative agreement with established plasma etching behaviors.

4 CONCLUSION

We have devised a feature-scale model for Cl_2/Ar inductively coupled plasma etching of titanium nitride (TiN) while replacing arriving particle fluxes with chamber settings. The model is implemented in the in-house open-source simulation tool ViennaPS, which uses a level set surface description and top-down Monte Carlo ray tracing to calculate the local arriving particle fluxes. Typical feature-scale simulations are based on parameters which are disconnected from the chamber inputs because a multi-scale simulation of the plasma chamber followed by a feature-scale simulation of the features is too time-intensive and prone to computational errors and convergence issues.

To overcome the limitations of the multi-scale reactor-and-feature combined simulation approach, we have simulated a broad range of chamber conditions while varying the critical inputs, such as the coil power, gas flow rate, chlorine and argon concentrations, chamber pressure, temperature, and applied bias voltage.

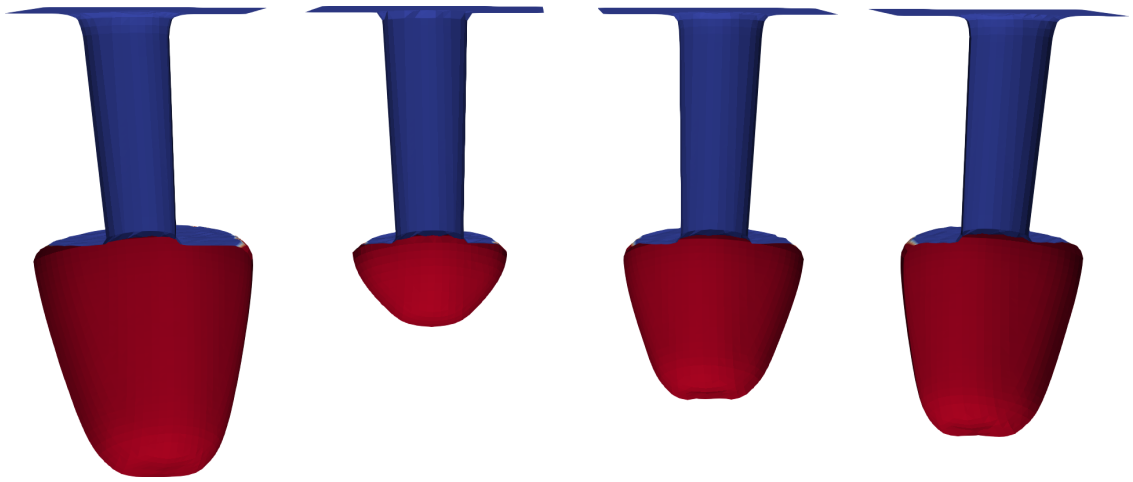

Figure 6: Etched profiles through a cylindrical hole SiO_2 mask (blue) for the plasma chamber settings provided in Table 2 which were chosen at random. The red layer depicts the etched TiN film.

In total 18 750 different combinations of the inputs have been carried out. The resulting fluxes from these simulations were used to build a six-dimensional hypercube, which can then be straightforwardly used by the feature-scale model to replace the ion and radical flux inputs with realistic chamber conditions.

ACKNOWLEDGMENTS

The financial support by the Austrian Federal Ministry of Labour and Economy, the National Foundation for Research, Technology and Development and the Christian Doppler Research Association, Austria is gratefully acknowledged. This research was also funded in whole or in part by the Austrian Science Fund (FWF) [10.55776/P35318].

REFERENCES

Alao, A. A., W.-N. Wu, and W.-D. Hsu. 2022. "Sticking Coefficient and Si/C Ratio of Silicon Carbide Growth Species on Reconstructed 4H-SiC(000$\bar{1}$) Surface by *Ab-initio* Calculations". *Vacuum* 205:111414.

Bloomenthal, J., C. Bajaj, J. Blinn, M.-P. Cani, B. Wyvill, A. Rockwood *et al*. 1997. *Introduction to Implicit Surfaces*. San Francisco, California: Morgan Kaufmann Publishers, Inc.

Bobinac, J., T. Reiter, J. Piso, X. Klemenschits, O. Baumgartner, Z. Stanojevic *et al*. 2023. "Effect of Mask Geometry Variation on Plasma Etching Profiles". *Micromachines* 14(3):665.

Carbone, E., W. Graef, G. Hagelaar, D. Boer, M. M. Hopkins, J. C. Stephens *et al*. 2021. "Data Needs for Modeling Low-Temperature Non-Equilibrium Plasmas: The LXCat Project, History, Perspectives and a Tutorial". *Atoms* 9(1):16.

Chiu, H. K., T. L. Lin, Y. Hu, K. C. Leou, H. C. Lin, M. S. Tsai *et al*. 2001. "Characterization of Titanium Nitride Etch Rate and Selectivity to Silicon Dioxide in a Cl_2 Helicon-Wave Plasma". *Journal of Vacuum Science & Technology A: Vacuum, Surfaces, and Films* 19(2):455–459.

Cooperberg, D. J., V. Vahedi, and R. A. Gottscho. 2002. "Semiempirical Profile Simulation of Aluminum Etching in a Cl_2/BCl_3 plasma". *Journal of Vacuum Science & Technology A: Vacuum, Surfaces, and Films* 20(5):1536–1556.

Donnelly, V. M. and A. Kornblit. 2013. "Plasma Etching: Yesterday, Today, and Tomorrow". *Journal of Vacuum Science & Technology A: Vacuum, Surfaces, and Films* 31(5):050825.

Ertl, O. 2010. *Numerical Methods for Topography Simulation*. Ph.D. thesis, Technische Universität Wien (TU Wien), Vienna, Austria. https://doi.org/10.34726/HSS.2010.001, accessed 16th September 2024.

Ertl, O. and S. Selberherr. 2009. "A Fast Level Set Framework for Large Three-Dimensional Topography Simulations". *Computer Physics Communications* 180(8):1242–1250.

Greenwood, J. 2002. "The Correct and Incorrect Generation of a Cosine Distribution of Scattered Particles for Monte-Carlo Modelling of Vacuum Systems". *Vacuum* 67(2):217–222.

Grujicic, M. and S. G. Lai. 2001. "Multi-Length Scale Modeling of Chemical Vapor Deposition of Titanium Nitride Coatings". *Journal of Materials Science* 36(12):2937–2953.

Hori, M. 2022. "Radical-Controlled Plasma Processes". *Reviews of Modern Plasma Physics* 6(36):1–117.

Huang, Y., C. Lin, Z.-H. Ye, Q.-J. Liao, and R.-J. Ding. 2015. "CH_4/Ar/H_2/SF_6 Plasma Etching for Surface Oxide Removal of Indium Bumps". *Journal of Electronic Materials* 44(7):2467–2472.

Huff, M. 2021. "Recent Advances in Reactive Ion Etching and Applications of High-Aspect-Ratio Microfabrication". *Micromachines* 12(8):991.

Kim, D.-P., J.-C. Woo, K.-H. Baek, K.-S. Park, K. Lee, K.-S. Kim *et al*. 2011. "Dry Etching of TiN in N_2/Cl_2/Ar Adaptively Coupled Plasma". *Vacuum* 86(4):380–385.

Klein, E. J. and W. F. Ramirez. 2000. "Consideration of Local Shadowing and Ion Beam Voltage Effects in the Prediction of a Surface Evolving Under Ion Milling". *Journal of Vacuum Science & Technology A: Vacuum, Surfaces, and Films* 18(1):166–175.

Klemenschits, X. 2022. *Emulation and Simulation of Microelectronic Fabrication Processes*. Ph.D. thesis, Technische Universität Wien (TU Wien), Vienna, Austria. https://doi.org/10.34726/hss.2022.89324, accessed 16th September 2024.

Klemenschits, X., S. Selberherr, and L. Filipovic. 2018. "Modeling of Gate Stack Patterning for Advanced Technology Nodes: A Review". *Micromachines* 9(12):631.

Krüger, F., H. Lee, S. K. Nam, and M. J. Kushner. 2024. "Voltage Waveform Tailoring for High Aspect Ratio Plasma Etching of SiO_2 Using Ar/CF_4/O_2 Mixtures: Consequences of Low Fundamental Frequency Biases". *Physics of Plasmas* 31(3):033508.

Lee Sang, B., M.-J. Gour, M. Darnon, S. Ecoffey, A. Jaouad, B. Sadani *et al*. 2015. "Selective Dry Etching of TiN Nanostructures Over SiO_2 Nanotrenches Using a Cl_2/Ar/N_2 Inductively Coupled Plasma". *Journal of Vacuum Science & Technology B, Nanotechnology and Microelectronics: Materials, Processing, Measurement, and Phenomena* 34(2):02M102.

Manstetten, P., L. Filipovic, A. Hössinger, J. Weinbub, and S. Selberherr. 2017. "Framework to Model Neutral Particle Flux in Convex High Aspect Ratio Structures Using One-Dimensional Radiosity". *Solid-State Electronics* 128:141–147.

Matsunami, N., Y. Yamamura, Y. Itikawa, N. Itoh, Y. Kazumata, S. Miyagawa *et al*. 1984. "Energy Dependence of the Ion-Induced Sputtering Yields of Monatomic Solids". *Atomic Data and Nuclear Data Tables* 31(1):1–80.

Osher, S. and J. A. Sethian. 1988. "Fronts Propagating with Curvature-Dependent Speed: Algorithms Based on Hamilton-Jacobi Formulations". *Journal of Computational Physics* 79(1):12–49.

Osher, S. and C.-W. Shu. 1991. "High-order Esentially Nonoscillatory Schemes for Hamilton-Jacobi Equations". *SIAM Journal on Numerical Analysis* 28(4):907–922.

Osipov, A. A., N. A. Andrianov, A. B. Speshilova, A. E. Gagaeva, S. Risquez, A. Vorobyev *et al*. 2023. "Highly Selective Plasma Etching Technique for Molybdenum". *Plasma Chemistry and Plasma Processing* 43(3):697–707.

Panagopoulos, T. and D. J. Economou. 1999. "Plasma Sheath Model and Ion Energy Distribution for All Radio Frequencies". *Journal of Applied Physics* 85(7):3435–3443.

Reiter, T., L. F. Aguinsky, F. Rodrigues, J. Weinbub, A. Hössinger, and L. Filipovic. 2024. "Modeling the Impact of Incomplete Conformality During Atomic Layer Processing". *Solid-State Electronics* 211:108816.

Reiter, T., N. Karnel, and L. Filipovic. 2024. *ViennaPS 2.0.0*. https://github.com/ViennaTools/ViennaPS/releases/tag/2.0.0, accessed 8th April, 2024.

Reiter, T., X. Klemenschits, N. Karnel, and L. Filipovic. 2024a. *ViennaLS 3.1.0*. https://github.com/ViennaTools/ViennaLS/releases/tag/v3.1.0, accessed 8th April, 2024.

Reiter, T., X. Klemenschits, N. Karnel, and L. Filipovic. 2024b. *ViennaRay 2.1.0*. https://github.com/ViennaTools/ViennaRay/releases/tag/v2.0.1, accessed 8th April, 2024.

Sethian, J. A. 1999. *Level Set Methods and Fast Marching Methods*. 2nd ed. Cambridge, UK: Cambridge University Press.

Shumilov, A. S., I. I. Amirov, and V. F. Lukichev. 2016. "Modeling of the High Aspect Groove Etching in Si in a Cl_2/Ar Mixture Plasma". *Russian Microelectronics* 45(3):167–179.

SIGLO database 2023. *LXCat 6.2*. https://fr.lxcat.net/home/, accessed 12th December, 2023.

Silbey, R. J., R. A. Alberty, G. A. Papadantonakis, and M. G. Bawendi. 2022. *Physical Chemistry*. 5th ed. Hoboken, New Jersey: John Wiley & Sons.

Steinbrüchel, C. 1989. "Universal Energy Dependence of Physical and Ion-Enhanced Chemical Etch Yields at Low Ion Energy". *Applied Physics Letters* 55(19):1960–1962.

Tonotani, J., T. Iwamoto, F. Sato, K. Hattori, S. Ohmi, and H. Iwai. 2003. "Dry Etching Characteristics of TiN Film Using Ar/CHF_3, Ar/Cl_2, and Ar/BCl_3 Gas Chemistries in an Inductively Coupled Plasma". *Journal of Vacuum Science & Technology B: Microelectronics and Nanometer Structures Processing, Measurement, and Phenomena* 21(5):2163–2168.

Woo, J.-C., D.-P. Kim, and G.-H. Kim. 2022. "Etch Mechanism of AlN Thin Film in Cl_2/Ar Inductively Coupled Plasma". *Transactions on Electrical and Electronic Materials* 23(5):569–577.

Woo, J.-C., S.-H. Kim, and C.-I. Kim. 2011. "Etch Characteristics of TiN/Al_2O_3 Thin Film by Using a Cl_2/Ar Adaptive Coupled Plasma". *Vacuum* 86(4):403–408.

AUTHOR BIOGRAPHIES

LADO FILIPOVIC is an Associate Professor and the Director of the Christian Doppler Laboratory for Multi-Scale Process Modeling of Semiconductor Devices and Sensors at the Institute for Microelectronics, TU Wien. Lado's research is centered around Integrated Semiconductor Sensors and Process Technology Computer Aided Design (TCAD). He obtained his *venia docendi* (habilitation) in Semiconductor Based Integrated Sensors and his doctoral degree (Dr.techn.) in Microelectronics from TU Wien. Lado is currently heading several research projects funded by the Austrian Science Fund (FWF), the Christian Doppler Forschungsgesellschaft (CDG), the European Union (EU), and industry. He is a Senior Member of the IEEE and is an active member of the TCP for many outstanding IEEE sponsored conferences. He is a reviewer for several funding agencies and many leading journals. His research team has released open-source scientific software tools under the ViennaTools moniker, such as ViennaPS and ViennaEMC, which have been applied for studying the fabrication and operation of advanced nanoelectronic devices. His email address is filipovic@iue.tuwien.ac.at and his website is https://www.iue.tuwien.ac.at/staff/filipovic/.

TOBIAS REITER is a doctoral candidate at TU Wien. He obtained his Master's degree (Dipl.-Ing.) in Technical Physics in 2022 and is currently completing the inter-faculty Master Program (MSc.) Computational Science and Engineering, both at TU Wien. He joined the Institute for Microelectronics, TU Wien as a doctoral candidate in 2022, where he is working on semiconductor process simulation. His current research focuses on the development of the process simulation library ViennaPS, where he is developing models for novel etching and deposition processes for semiconductor fabrication. He is also part of the Christian Doppler Laboratory for Multi-Scale Process Modeling of Semiconductors Devices and Sensors. His email address is reiter@iue.tuwien.ac.at and his website is https://www.iue.tuwien.ac.at/staff/reiter/.